Materials Chemistry and Physics 319 (2024) 129303

Contents lists available at ScienceDirect

Materials Chemistry and Physics

journal homepage: www.elsevier.com/locate/matchemphys

Microstructural analysis of additively manufactured Ti–6Al–4V subjected to duplex surface treatment

Kelsey Ann Vella [a], Joseph Buhagiar [a], Glenn Cassar [a], Bonnie Attard [a], Jian Chen [b], Ann Zammit [a,*]

[a] Department of Metallurgy and Materials Engineering, Faculty of Engineering, University of Malta, Msida, MSD 2080, Malta
[b] School of Materials Science and Engineering, Southeast University, Nanjing, 211189, China

HIGHLIGHTS

- Advancing additive manufacturing and surface treatment for improved performance.
- Duplex treatment to enhance additively manufactured Ti64 substrates.
- Shot peening mitigates the tensile stresses and negative effect of build defects.
- Shot peening enhances the PVD coating's load-bearing capabilities.

ARTICLE INFO

Keywords:
Shot peening
PVD coating
Residual stress
Ti–6Al–4V
Laser powder bed fusion
Additive manufacturing
Duplex surface engineering

ABSTRACT

In this research, the impact of an innovative duplex surface treatment on the surface characteristics of additively manufactured Ti–6Al–4V was investigated. This duplex approach encompasses two distinct stages; the material is initially subjected to mechanical shot peening, followed by the application of a ceramic multilayer coating (consisting of Ti, TiN, TiAlN and TiAlCuN) through physical vapor deposition. The comprehensive analysis delves into the influence of the shot peening procedure, employing advanced techniques such as X-ray diffraction stress measurements, profile hardness assessments, and electron backscatter diffraction. The mechanical shot peening treatment induced a hardened surface layer, approximately 150 μm thick. This transformation was accompanied by the generation of compressive residual stresses, detected up to depths of 150 μm from the surface. Notably, the most substantial compressive residual stress, measuring 770 MPa, is located at a depth of approximately 27 μm beneath the surface. The existence of these stresses is further substantiated by average misorientation measurements of the cross-sections. The duplex treatment led to a remarkable advancement in the material's microhardness, exhibiting an increase of approximately 210% when compared to the untreated sample. Additionally, the ceramic coating itself demonstrates outstanding mechanical properties, with a nanohardness of 26 GPa, and an elasticity index (H/E) of 0.08. Furthermore, when subjected to scratch tests, the duplex-treated specimens exhibited enhanced durability attributed to the concurrent rise in surface roughness induced by the peening process.

1. Introduction

Titanium alloy Ti–6Al–4V (Ti64) has a longstanding presence in various industries due to its desirable properties. Its popularity is growing in marine applications owing to its impressive specific strength, fatigue and corrosion resistance, while also significantly reducing weight compared to traditional marine materials [1–3]. Despite its high manufacturing costs and energy requirements, these drawbacks are offset by its prolonged service life and reduced maintenance expenses [4].

This study addresses the substitution of conventionally wrought Ti64 with additively manufactured (AM) Ti64. Although widely used in other sectors, additive manufacturing remains emergent in marine applications. Laser powder bed fusion (L-PBF) is used to create this alloy, enabling the fabrication of intricate components that are challenging or impossible to produce conventionally. This approach reduces

* Corresponding author.
E-mail address: ann.zammit@um.edu.mt (A. Zammit).

https://doi.org/10.1016/j.matchemphys.2024.129303
Received 23 October 2023; Received in revised form 25 January 2024; Accepted 3 April 2024
Available online 4 April 2024

production time and material waste by eliminating multiple manufacturing steps due to near net-shape fabrication route [5]. However, the process can lead to elevated tensile residual stresses and surface roughness, adversely impacting the fatigue, erosion, cavitation, and corrosion resistance necessary for marine purposes [5,6]. To counter these issues while enhancing material performance, a duplex treatment strategy is proposed, involving shot peening (SP) followed by the deposition of a ceramic multilayer coating via physical vapor deposition (PVD), supplemented by a prior heat treatment.

Typically, duplex post-processing treatments for AM metals involve a combination of heat treatment with other surface or bulk treatments. The heat treatment aims to homogenise the microstructure, alleviate induced tensile residual stresses, and eliminate anisotropy. It is often combined with techniques like hot isostatic pressing, sandblasting, or shot peening [7]. These treatments mitigate roughness, porosity, build defects, or tensile stresses induced during additive manufacturing by substituting them with compressive residual stresses. Shot peening also enhances fatigue resistance by inducing compressive stresses, reducing the pore size of any pores in the near-surface region, and enhancing wear resistance through increased hardness [8]. PVD coatings primarily aim to enhance the surface wear resistance and hardness, while also providing corrosion protection by acting as a barrier [9]. A duplex treatment is proposed to harness the benefits of both processes. Additionally, to enhance resistance against biofouling, copper ions are incorporated into the multilayer coating's final layer due to their antifouling properties [10].

Several studies have examined the impact of shot peening on wrought Ti–6Al–4V [11–15]. Ahmed et al. [12] observed increases in surface hardness up to 395 HV together with a 250 μm deep hardened layer, and a maximum compressive residual stress of 1096 MPa just beneath the surface following peening. Similar effects were observed for shot-peened L-PBF Ti64, with values varying based on the peening parameters used [15,16]. Zhang et al. [16], after shot peening L-PBF Ti64, noted a surface hardness of 416 HV, a maximum compressive residual stress of 806 MPa, and a 180 μm deep hardened layer.

Electron backscatter diffraction (EBSD) enables comparison of treatment effects on different microstructures; several researchers have employed this technique to investigate the effect of the shot peening treatment on grain size, orientation, and texture of wrought Ti64 [11,17,18]. Wrought Ti64 typically exhibits an equiaxed microstructure, whereas the microstructure of AM Ti64 is composed of fine elongated laths, resulting in different behaviour. Unlike laser shock peening effects on AM Ti64 [19–21], the effect of shot peening on AM Ti64 via EBSD analysis has not been extensively studied. This investigation aims to provide deeper insight into shot peening's effects by analysing changes in lath size distribution and misorientation values following the applied treatments.

While the combination of shot peening together with PVD coatings is relatively novel for AM Ti alloys, multiple studies have explored their impact on wrought Ti alloys. Shot peening has been shown to enhance adhesion of PVD coatings [22,23]. Zammit et al. [23] observed superior adhesion in shot-peened and WC/C coated wrought Ti64 compared to a coated-only condition, suggesting that the induced roughness does not compromise adhesion properties. Adhesion is crucial for load transfer in the coating-substrate system, and optimal performance necessitates strong adhesion typically achieved by coating a smooth surface [9]. Shot peening enhances surface roughness, encouraging mechanical bonding between the surface and the coating, however this phenomenon diminishes beyond a certain threshold. Additionally, the work-hardening from peening improves substrate deformation resistance, enhancing coating resistance to delamination by reducing the underlying deformation of the substrate upon application of a load [23,24].

To date, the impact of the proposed duplex treatment on additively manufactured Ti64 remains largely unexplored in literature. This study aims to provide a comprehensive analysis of how shot peening and PVD coating collaboratively impact the surface and near-surface characteristics of this material. An array of advanced characterisation techniques was employed, including electron backscatter diffraction (EBSD), X-ray diffraction (XRD), nano- and microhardness testing, as well as profilometry, to thoroughly investigate these effects. The outcomes of this research are anticipated to yield significant insights that can advance the fields of additive manufacturing and surface treatment of Ti64.

2. Materials and methods

Cylindrical samples were generated employing an AmPro Innovations SP100 Metal 3D Printer (China) laser powder bed fusion system. The coupons, having a 20 mm diameter and 6 mm thickness, were fabricated from Ti–6Al–4V powder with particle diameters ranging from 15 to 53 μm. Key processing parameters included a laser power of 100 W, laser speed of 600 mms^{-1}, a layer thickness of 30 μm and a hatch spacing of 70 μm. Subsequently, the coupons underwent heat treatment in a nitrogen atmosphere at 800 °C for 2 h, followed by furnace cooling using a T.A.V. Dualjet TPH-200 (Italy) furnace. These heat treatment parameters were chosen with the aim of relieving tensile stresses whilst ensuring the breakdown of the brittle acicular martensite phase, without inducing significant grain growth and thus retaining the material's strength. The samples were then ground and polished using standard metallographic techniques up to a mean surface roughness, R_a, equivalent to ~45 nm.

Shot peening was performed using an Industrial Surface Treatment Ltd. AB850 air blasting machine, comprising an 80 mm-long nozzle with an inner diameter of 6 mm. The shot peening process incorporated an Almen intensity of 20 mmA, a pressure of 7 bar and a working distance of 100 mm. Zirshot Z300 (France) shots, primarily composed of ZrO_2, SiO_2 and Al_2O_3, with a size distribution ranging from 300 to 450 μm, were utilised.

A multilayer coating, consisting of four distinct layers (Ti/TiN/TiAlN/TiAlCuN), was deposited by unbalanced magnetron sputtering (UDP800, Teer Coating Ltd., UK), using two Ti, one Al and one Cu targets. The deposition parameters are shown in Table 1. The specimen rotation speed was 4 rpm, while the deposition pressure was 0.23 Pa. The target-to-specimen distance was 145 mm. The deposition

Table 1
Deposition parameters for the PVD process.

Steps	Total time	Time	Bias voltage (V)	OEM[a] (%)	Target current (A)			
					1: Ti	2: Ti	3: Al	4: Cu
Clearing	10 min	0 Ramp 2 min Stable 8 min	200 400 400	0	0.5		/	/
Ti layer	15 min	0 Ramp 10 min Ramp 5 min	90	0	0.5 8		/	/
TiN layer	60 min	0 Ramp 30 min Stable 30 min	90	100 35	8		/	/
TiAlN layer	60 min	0 Ramp 5 min Stable 55 min	90	35	8		2 8	/
TiAlCuN layer	60 min	60 min	90	35	8		8	8

[a] OEM stands for the optical emission monitor system. Nitrogen flow was dynamically regulated according to the intensity of glow generated by the atoms on the surface of the Ti target.

temperature is from 25 °C to 180 °C.

Table 2 shows the nomenclature used to categorise the different sample conditions.

To assess the surface topography, an AEP Technology NanoMap-500LS (USA) contact profilometer was employed to obtain linear scans. Each line scan covered a 2500 μm distance at a scanning rate of 25 μms^{-1}, with a lateral resolution of 1 μm and a vertical resolution of 0.1 nm. Five scans were conducted at various positions to determine average roughness measurements.

Vickers microhardness measurements were carried out using a Mitutoyo MVK-H2 (Japan) hardness tester. A 100 gf load was applied for all measurements, with five indentations to establish surface hardness measurements repeated across the cross-section to create profile hardness measurements.

For in-depth analysis of the coating, a Carl Zeiss Merlin Gemini (Germany) scanning electron microscope (SEM) was utilised at high magnifications. Elemental analysis was conducted out using SEM in combination with an Ametek EDAX (USA) energy dispersive spectroscopy (EDS) detector.

Nanohardness measurements were performed using a Nanomaterial NanoTest 600 (U.K.) instrument, which was outfitted with a Berkovich 120° diamond tip indenter and applying a maximum load of 50 mN. These measurements were conducted on a coating deposited on a metallographically polished wrought Ti–6Al–4V sample.

Scratch testing was performed using a Bruker UMT TriboLab (USA) machine, employing a 60° Rockwell C indenter. A total of five scratches were made per sample, each spaced 2 mm apart. The test parameters included a ramped load starting from 1 N to 40 N, a scratch length of 10 mm, a duration of 30 s and a scanning velocity of 0.33 mm s^{-1}. The scratch morphology was examined using a Carl Zeiss Axioscope 5 (Germany) optical microscope, and a Carl Zeiss Merlin Gemini (Germany) scanning electron microscope (SEM) to identify the critical loads (L_C) at which failure occurred, following EN ISO 20502:2016.

For phase analysis, a Bruker AXS D8 Advance (USA) diffractometer, utilising Bragg Brentano geometry, was deployed. Scans were conducted within a 2θ range of 20° to 90°, with a 0.02° step size and a 2 s dwell time. The Rigaku Ultima IV (Japan) diffractometer, configured in the Glancing Incidence Asymmetric Bragg (GIAB) mode, was used to analyse the coating, following the same parameters with an initial angle of 3°. Both diffractometers employed a CuKα radiation source operating at 45 kV acceleration voltage and 40 mA current.

Stress measurements were acquired using a Rigaku Ultima IV (Japan) diffractometer. The α-Ti (213) pyramidal plane peak was selected for peak shifting measurements, and scans were conducted across a 2θ range of 139° to 144°, using a 0.02° step size and a 5-s acquisition time. Measurements were taken at seven ψ tilts, ranging from 0° to 60°, with stresses calculated via the $Sin^2\psi$ method. Layer removal was performed using a Struers LectroPol-5 (Denmark) electropolishing machine, employing an electrolyte comprising 10% perchloric acid and 90% ethanol. The value of Young's Modulus used was 114 GPa which was obtained from tensile tests carried out on the material, while the Poisson's ratio used was 0.3.

For electron backscatter diffraction (EBSD) analysis, specimens were sectioned and metallographically polished to a mirror finish. EBSD measurements were conducted using Carl Zeiss Merlin Gemini SEM equipped with an EBSD/EDX Ametek (USA) detector. Scans covered a 290 μm by 240 μm with a 0.5 μm step size, a working distance between 12 and 14 mm, a working voltage of 20 kV and a probe current of 10 nA. Data analysis was carried out using OIM Analysis™ v8 software. Scans were filtered to exclude points with a confidence interval less than 0.1 and grain size of less than five points. Additionally, scans were processed using a grain dilation method ensuring that less than 10 % of the scan data was altered.

Table 2
Nomenclature used to categorise sample conditions.

Designation	L-PBF	Heat treatment	Polished	Shot peened	PVD Coated
AB	✓				
HT	✓	✓	✓		
SP	✓	✓	✓	✓	
PVD	✓	✓	✓		✓
DU	✓	✓	✓	✓	✓

3. Results and discussion

3.1. Analysis of the surface morphology

In Fig. 1, the mean roughness (R_a) and mean maximum height (R_z) values were observed to be similar for the as-built and heat-treated (HT) and coated-only (PVD) substrates. However, an increase of a magnitude of ~30, becomes evident in the case of the shot peened (SP) and duplex-treated (DU) conditions. This increase in surface roughness can be attributed to the peening treatment's effects, as the impacting shots induce surface deformation and the formation of dimples characteristic to the process. The extent of surface roughening is intricately linked to the intensity of the peening process, whereas the maximum depth of dimple achieved is directly influenced by the diameter of the shot particles employed [16]. Furthermore, it is worth noting that the deposited coating reflects the underlying rough surface morphologies, resulting in a highly conformal coating. This behaviour can be attributed to the light-of-sight deposition characteristics of magnetron sputtering. It is good to note that, in certain cases, the smoothing of the coating may not be the preferred outcome as there is a potential consequence of achieving a shallow coating thickness at surface asperities, which, in turn, could promote crack initiation through fragmentation mechanisms [25].

3.2. Analysis of the hardness

The hardness measured on the AB sample was 346 HV, while after heat treatment the hardness decreased to 332 HV. This can be attributed to the phase transformation from α' to α and β, which is softer. After subjecting the material to surface engineering treatments, significant improvements in microhardness were observed, with a 13% increase for SP conditions and a 210% increase for the DU conditions. This increase in hardness can be primarily attributed to the induced work hardening resulting from the peening treatment. While the treatment has the potential to induce a martensitic transformation that contributes to further hardening, the investigations, as confirmed by XRD phase analysis in Section 3.4, revealed that such transformation did not occur in this case. This non-occurrence aligns with prior research on Ti alloys, where the small crystal lattice distortion makes the transformation unlikely [26].

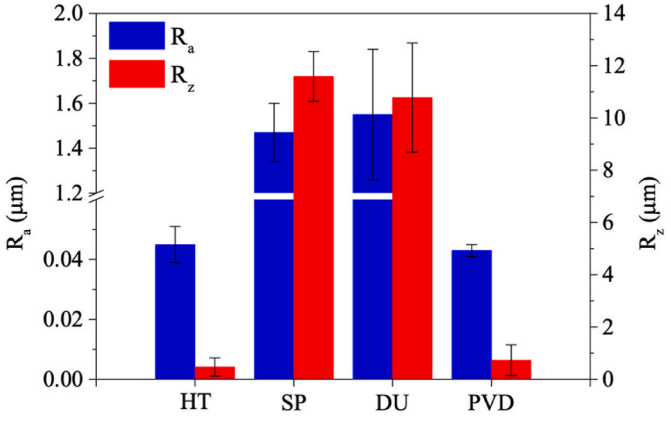

Fig. 1. Surface roughness measurements obtained for all sample conditions.

The examination also unveiled the formation of a robust hardened layer approximately 150 μm below the surface, as depicted in Fig. 2. It is worth noting that the literature reports variations in hardening depths, contingent on peening parameters and the microstructure under treatment. Increased peening duration, intensity and shot size typically promote greater hardening depths [12,27]. The deposition of a coating onto a hardened, shot peened surface holds notable advantages. A harder substrate enhances the load-bearing capabilities of the coating mitigating stress concentration at the substrate-coating interface and thereby extending the service life of coatings in harsh environments [28,29]. Additionally, the multilayer structure of the coating contributes to the improved load-bearing capabilities, as the various layers further impede dislocation movement [30].

3.3. Analysis of the coating

Fig. 3 shows the coating's dense and characteristic columnar structure typical of titanium nitride coatings [30]. The successive deposition of distinct layers effectively interrupts the growth of these columnar grains, leading to a denser coating with reduced grain size, in agreement with the findings of Çomakli et al. [30]. Overall, the coating has an average thickness of 4.26 μm, with individual layer thicknesses as follows: (i) Ti: 0.35 μm; (ii) TiN: 1.25 μm; (iii) TiAlN: 1.80 μm; and (iv) TiAlCuN: 0.86 μm. This multilayer structure not only enhances mechanical properties but also contributes to an improved corrosion resistance by impeding the transportation of corrosive media through coating defects typical of columnar structures [30]. Analysis of the cross-sections of the coating revealed no sub-surface cracks, thus over-peening did not occur.

Table 3 presents the nanoindentation results, encompassing hardness, modulus of elasticity and elasticity index of the coating. A 50 mN load resulted in a maximum indentation depth of approximately 336 nm, which is less than 10% of the total coating thickness. These findings align with previous studies by Feng et al. [31] who obtained a hardness equivalent to 24.52 GPa for a Ti–Al–Cu–N monolayer coating having 1.07 at% Cu, whilst Belov et al. [32] observed a hardness equivalent to 22 GPa which increased up to 49 GPa when having 3.05 at% Cu. The high elasticity index obtained signifies the coating's ability to absorb elastic deformation without failure, making it resistant to crack initiation under cyclic stresses [11]. Therefore, the application of the coating is deemed advantageous, as it exhibits a higher index compared to the untreated sample.

To delve deeper into the coating's characteristics, two sample conditions, duplex-treated (DU) and coated-only (PVD) substrate, were subjected to scratch testing. Figs. 4 and 5 provide detailed insights into the observed characteristics following these tests. High-magnification micrographs in Fig. 5 suggest that while the DU sample exhibited less distinct scratching, it suffered comparatively more damage toward the end of the scratch, eventually leading to complete delamination.

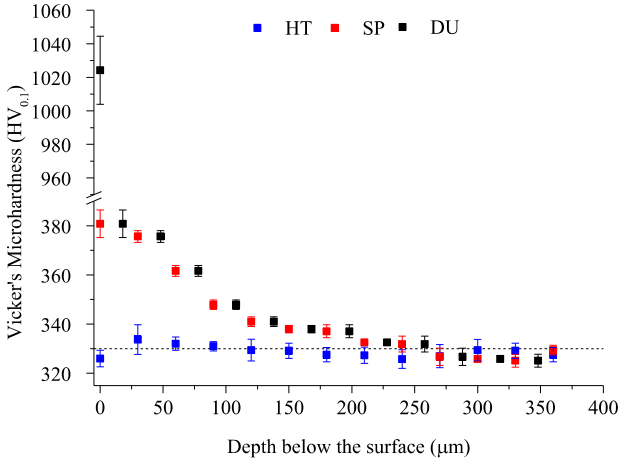

Fig. 2. Vickers microhardness surface and profile measurements.

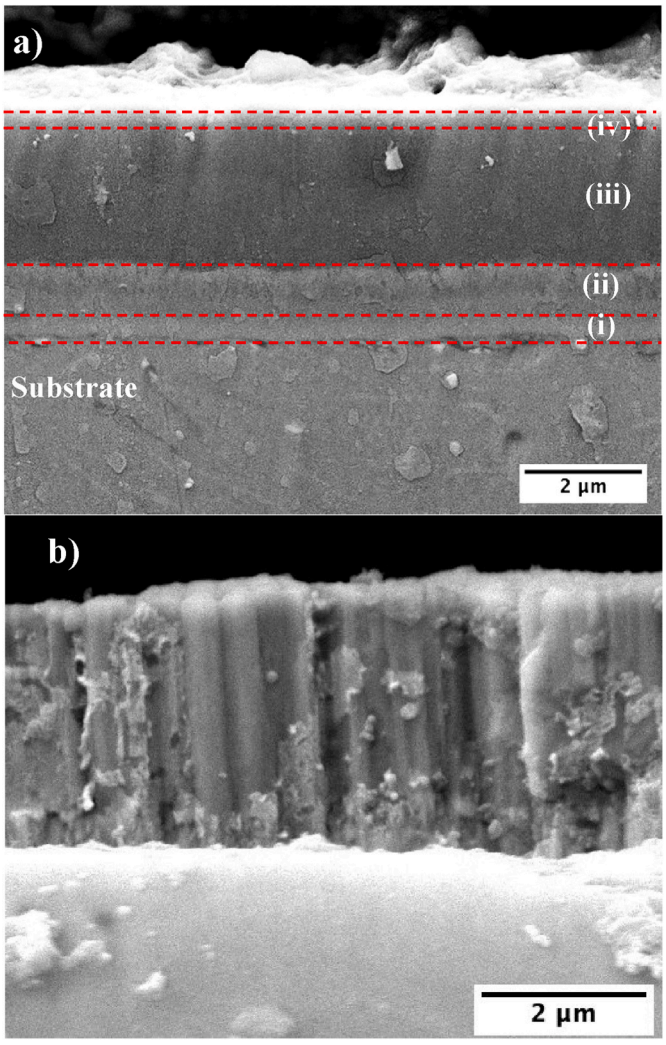

Fig. 3. High magnification micrographs depicting a) the various layers of the multilayer coating and b) a fractured section of the coating showing the coating's columnar structure.

Table 3
Data obtained from nanohardness testing of the multilayer coating compared with the data of printed and heat-treated Ti–6Al–4V.

	Hardness, H (GPa)	Modulus of Elasticity, E (GPa)	Elasticity Index, H/E
HT	3.00 ± 0.03	99 ± 3	0.030 ± 0.001
PVD	26.00 ± 2.00	337 ± 38	0.080 ± 0.011

For the DU-treated sample, the very rough surface impeded the clear visualisation of L_{C1} (the start of chevron cracking in the coating), but this does not necessarily indicate an absence of chevron cracks. Both sample conditions exhibited L_{C2} characteristics (chipping failure on the edges of a scratch track), while no L_{C3} (delamination of the coating within the scratch track) was observed for the PVD-only sample. This suggests superior coating adhesion when applied to a polished untreated alloy compared to that deposited on a shot-peened surface. Evidently, the DU samples experienced continuous coating removal at a normal load of 33 N, which was not apparent in the PVD sample. The variance in performance can be ascribed to the increased roughness of the DU sample,

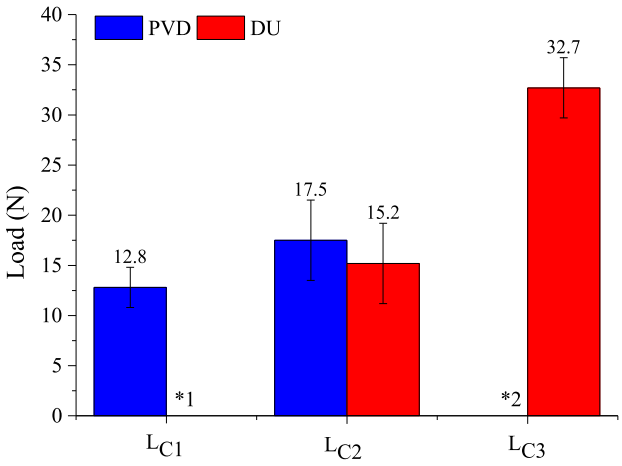

Fig. 4. Bar graph of critical loads sustained by each sample (L_{C1} is characterized by the start of chevron cracking in the coating, L_{C2} by chipping failure on the edges of the scratch track, and L_{C3} by delamination of the coating within the scratch track). *1 No values were obtained for L_{C1} on the DU sample, since these characteristics were difficult to identify on the roughened surface. *2 No values were obtained for L_{C3} as the PVD coated only substrate sustained no such damage.

altering the interaction between the tip and the surface and encouraging a higher defect density during deposition, leading to a loss in local adhesion [9].

However, it is worth noting that the substrate's initial hardness also plays a significant role. Comparatively, the AM Ti64 substrate exhibited higher hardness and less roughness than the AM 316L SS substrate reported by Bonnici et al. [33]. In particular, the AM Ti64 substrate proved to be 46% and 12% harder than AM 316L SS in the untreated and shot-peened conditions, respectively. Consequently, the harder and smoother AM Ti64 substrate facilitated load-carrying capabilities for the coating, as evidenced by its enhanced performance compared to the softer AM 316L SS substrate.

3.4. X-ray diffraction analysis

X-ray diffraction phase analysis, as presented in Fig. 6, provides crucial insights into the structural transformations within the material. In the as-built and heat-treated (HT) samples, the presence of a slight β-Ti(110) peak confirms the transformation from α' to α + β. Notably, the peaks in the HT sample exhibit a slight shift towards lower 2θ values when compared to the standard powder diffraction files of hcp α-Ti and bcc β-Ti. This shift can be attributed to the heat treatment process, which alters the crystal parameters due to the diffusion of solute atoms, resulting in lattice expansion and increased parameter values [34].

Similarly, a shift towards lower 2θ values is observed for the as-built and shot peened (SP) sample, alongside broader and less intense peaks. These changes can be attributed to the increased surface roughness, where surface asperities absorb diffracted rays, thus altering the diffraction spectra [11] while the shift is a consequence of the induced compressive residual stresses. No new reflections were detected in this study, indicating that phase transformation due to SP did not occur, likely due to the relatively low peening intensity employed.

For the duplex-treated (DU) sample, as with the SP sample, peak broadening and differences in intensity compared to the coated-only (PVD) sample were observed. These differences can be attributed to the surface condition of the prior shot peened DU sample. Both DU and

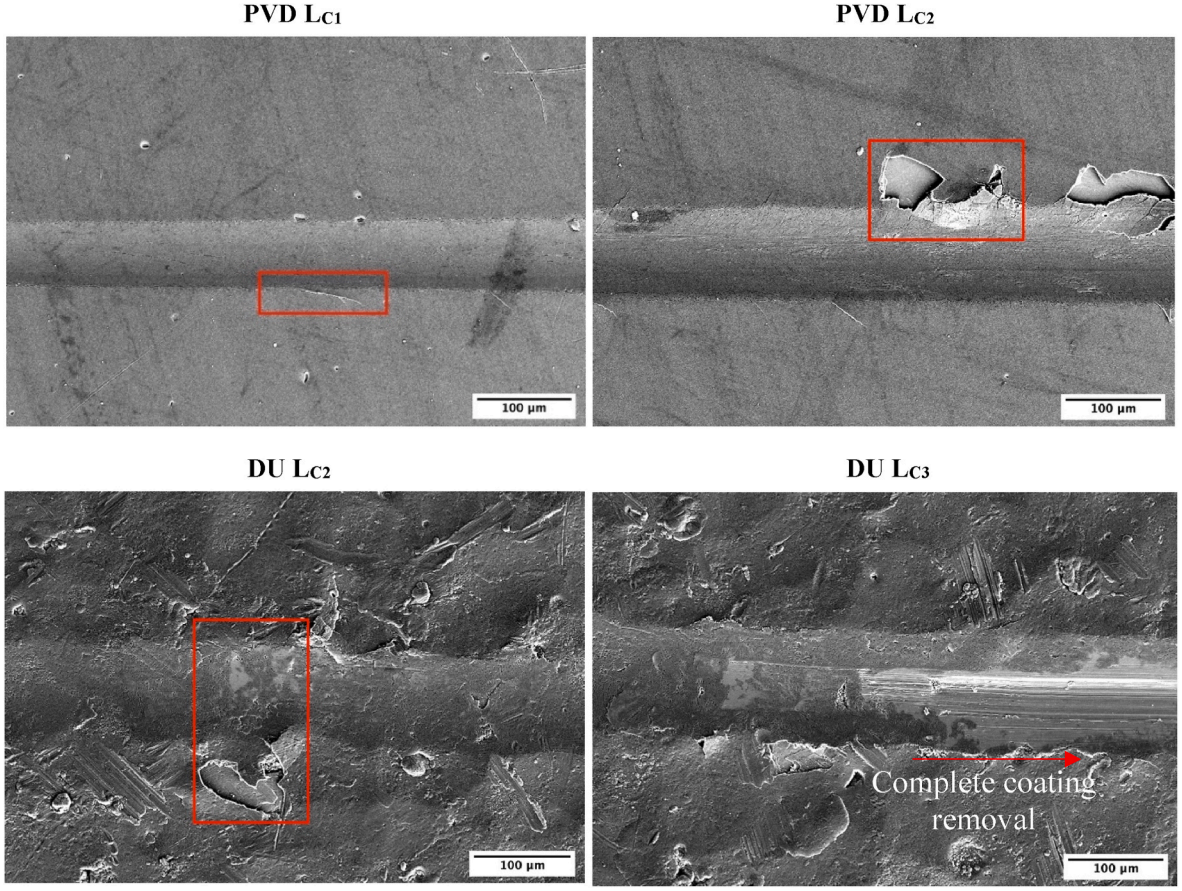

Fig. 5. High magnification micrograph of the various characteristics observed in the scratch tracks.

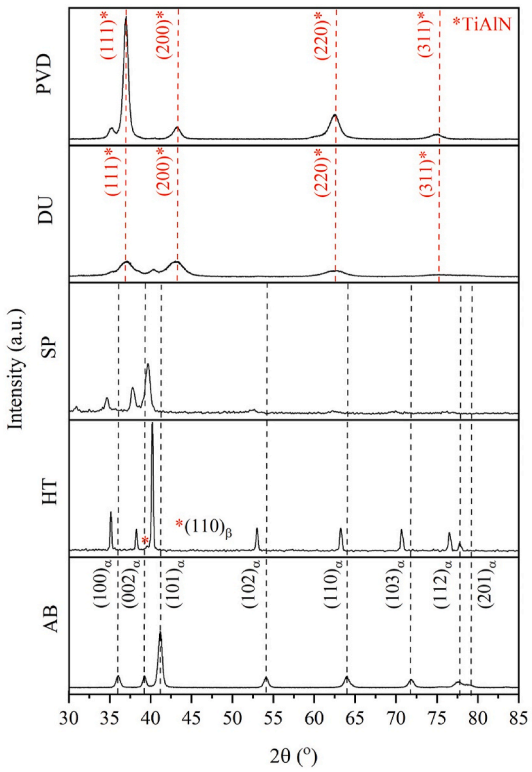

Fig. 6. X-ray diffraction peaks obtained for the different sample conditions.

PVD samples exhibited reflections along the (111), (200) and (220) planes, characteristic of TiN and TiAlN coatings [30]. No copper peaks were observed, suggesting either the Cu phases were not crystalline or not present in sufficient quantities to be detectable.

Fig. 7 illustrates the residual stresses observed at and below the surface for various sample conditions. Notably, the SP condition exhibited a compressive residual stress (CRS) of 744 MPa at the surface, indicating significant plastic deformation. A maximum CRS of 777 MPa was observed at a depth of 27 μm, consistent with findings by Zhang et al. [16] for L-PBF Ti64 following shot peening. The magnitude of the induced stresses is influenced by shot velocity and diameter, with higher

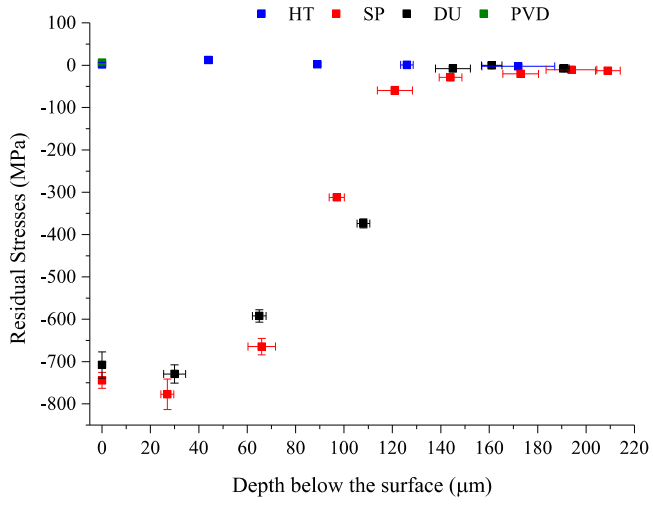

Fig. 7. Residual stress measurements obtained via x-ray diffraction for the different sample conditions. Residual stress errors were obtained via Gaussian error propagation, whilst depth errors were obtained by the min-max method. Measurements are along the build direction.

speeds inducing greater plastic deformation and increased surface CRS [16].

The DU condition displayed similar stress values to the SP condition, with a surface CRS of 708 MPa and a maximum CRS of 729 MPa at a depth of 30 μm. This indicates that the coating deposition process did not alleviate these residual stresses significantly. Beyond depths of 140–150 μm from the surface, residual stresses in both sample conditions were no longer compressive, correlating with the hardened layer's depth induced by the peening treatments, consistent with microhardness measurements. Conversely, the HT and PVD samples exhibited minor tensile residual stress at the surface, with values of 2 MPa and 6 MPa, respectively. These tensile stress levels are deemed insignificant, demonstrating the effectiveness of the heat treatment in relieving any substantial tensile residual stresses induced by the L-PBF process.

3.5. EBSD analysis

The grain size plots and misorientation maps obtained for the different conditions are depicted in Figs. 8 and 9, respectively, to comprehensively analyse the microstructure's response to the manufacturing process and surface treatments. The microstructure initially comprises columnar prior-β grains, which upon cooling during the L-PBF process transform into laths. The columnar growth parallel to the build direction is a hallmark of L-PBF and is driven by steep temperature gradients resulting from the heat flow toward the substrate, combined with epitaxial growth between layers from re-melting previously solidified layers [35]. Subsequently, these columnar grains undergo a diffusionless transformation to α′ lath colonies upon rapid cooling, as demonstrated in Fig. 9(a) for the as-built (AB) condition [36].

Given the thin and elongated lath morphology, grain diameter

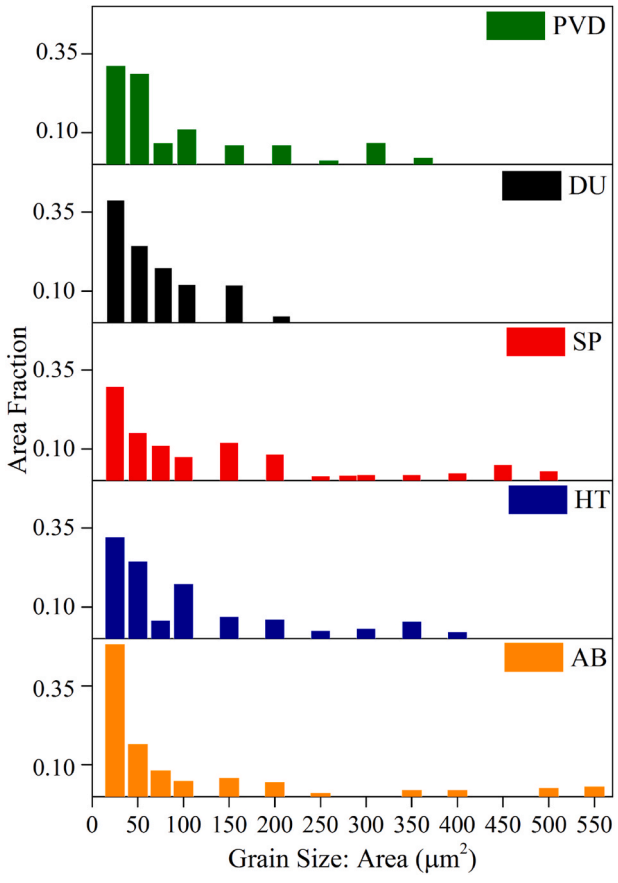

Fig. 8. Relationship between grain size (in terms of area) and area fraction across various sample conditions, as determined through EBSD measurements.

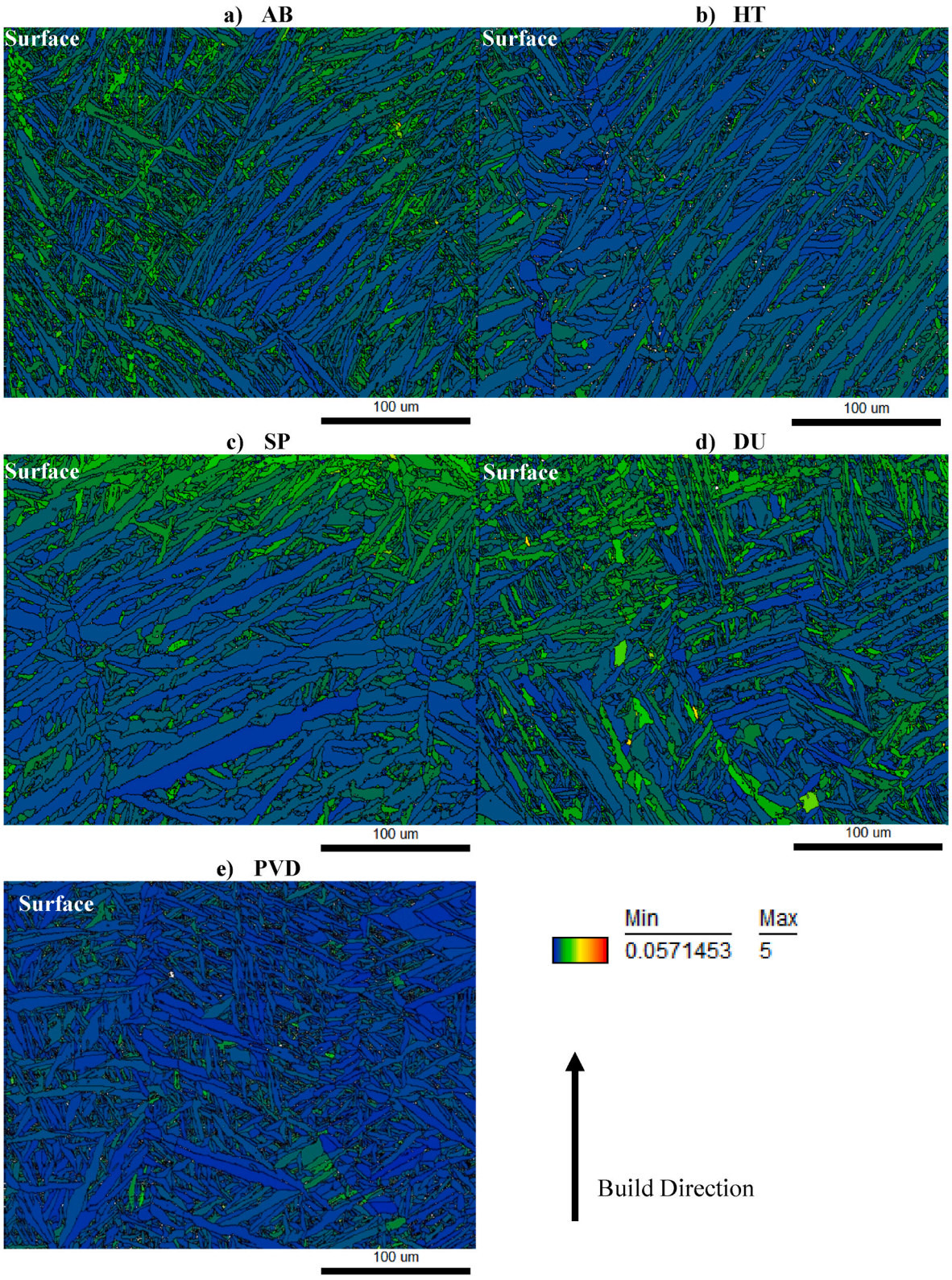

Fig. 9. Grain average misorientation maps for cross-sections of the different conditions, obtained along the cross-section up to depths of 240 μm from the surface.

measurements prove inaccurate for grain size analysis. Hence, grain area measurements were utilised in this study. Grain area was plotted against area fraction values for various sample conditions (Fig. 8) within a near-surface area of approximately 290 μm by 100 μm. Due to the wide range of lath sizes observed, common after AM processes due to varying thermal gradients throughout the specimens, significant overlap in measurements occurred. Following heat treatment, the lath structure remained intact (as shown in Fig. 9(b)).

The SP treatment did not lead to significant lath refinement as indicated in Fig. 8, a finding in line with Hu et al.'s observations [37] for laser peened direct laser deposited Ti64. The pre-existing fine micro-structure prior to peening may contribute to this result. Yeo et al. [20]

note a slight decrease in average grain size following laser shock peening of L-PBF Ti64, though their work showed some statistical overlap in values. Similarly, in this study, significant statistical overlap in measurements suggests that any refinement, if present, was slight and not statistically significant.

Aspect ratios for the near-surface microstructures are provided in Table 4, indicating a slight decrease in aspect ratios for the SP and DU samples compared to the heat-treated specimens. This suggests a potential shift from an elongated to a more globular shape, albeit with minimal change within the limits of statistical uncertainty. Grain refinement in hcp materials via severe plastic deformation techniques is challenging due to the structure's high deformation resistance [38]. Plastic deformation triggers dislocation generation and motion, with accumulated dislocations eventually becoming immobile, leading to grain refinement as low-angle grain boundaries transform into high-angle grain boundaries [11]. An initial fine microstructure inhibits dislocation mobility, necessitating exceedingly high peening intensities for significant grain refinement.

Misorientation measurements were used to examine the effect of shot peening. Fig. 9 compares grain average misorientation (GAM) maps for different conditions. An increase in the degree of local misorientation is expected to occur due to localised stress application from the SP process and residual stresses from the additive manufacturing process. Local average misorientation measurements within a crystal structure can be correlated with geometrically necessary dislocations (GNDs), whereby an increase in misorientation can indicate an increase in GNDs [39,40]. The as-built (AB) sample in fact, exhibited significant misorientation distributed across the cross-section, attributed to tensile residual stresses induced by the steep thermal gradients during L-PBF. Following heat treatment, as expected, misorientation values significantly decreased.

In contrast, both shot-peened (SP) and duplex treated (DU) conditions exhibited substantial misorientation levels at the surface, attributable to induced compressive residual stresses from shot peening. GNDs can introduced through strain hardening processes such as shot peening, thus resulting in an increase in the misorientation measurements observed near the surface and a decrease as one moves to the interior of the specimen. This increased measurable misorientation values extended to a depth of approximately 100 μm beneath the surface, corroborating stress and hardness measurements of the near-surface area. No evidence of twinning, a typical mechanism in hcp crystals, was observed, possibly due to factors such as small initial grain size, insufficiently high peening intensity and a high Al content suppressing twin formation [17,41,42].

To quantitatively assess the induced stresses, the Kernel Average Misorientations (KAM) along the depth from the surface were plotted, as shown in Fig. 10. Upon heat treatment, the KAM value decreased from 0.76 to 0.67, reflecting stress relief caused by the heat treatment. However, the SP and DU samples exhibited a rise in KAM near the surface, indicating localised strain concentration and induced residual compressive stress [20]. These induced stresses and plastic deformation from the SP process would have led to an increase in dislocation density resulting in a change in grain orientation near the surface. The rotation of laths is attributed to dislocation movement within the lattice, contributing to the elevated KAM values in the near-surface area.

Table 4
Aspect ratio measurements across different sample conditions as determined through EBSD measurements with a resolution of 0.5 μm.

Sample Condition	Aspect Ratio
AB	3.37
HT	3.68
SP	3.27
DU	2.90
PVD	3.60

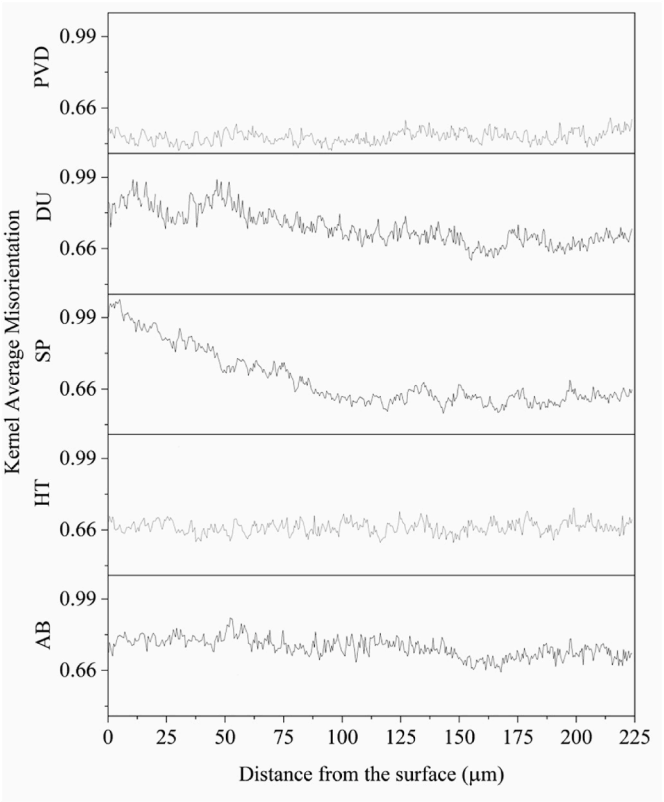

Fig. 10. Kernel Average Misorientation measurements along the depth for the different sample conditions.

3.6. Summary

The results presented in the previous sections explore the surface morphology, hardness, coating characteristics, X-ray diffraction analysis and microstructure of a Ti–6Al–4V titanium alloy subjected to various treatments, including shot peening and a duplex treatment. The following section summarises the key findings.

A comprehensive analysis, employing a range of characterisation techniques on duplex treated additively manufactured Ti64 titanium alloy, including X-ray diffraction and electron backscatter diffraction analysis was carried out. The following key findings were obtained:

1. The duplex treatment led to a remarkable 210% increase in hardness attributed to a combination of factors, namely, the introduction of compressive residual stresses, and the inherent high hardness of the multilayer coating, having a nanohardness of 26 GPa. This treatment resulted in the formation of a hardened layer ~150 μm deep.
2. The PVD coating exhibited very good adhesion characteristics, particularly on smooth polished surfaces, where it demonstrated high resistance to large normal loads. The introduction of surface roughness through the peening process was not conducive to mechanical interlocking.
3. The peening treatment did not induce any phase transformation; but did generate significant compressive residual stresses, detectable up to a depth of 150 μm. While some evidence of grain refinement was observed, it was minimal due to already fine initial microstructure.
4. The deposition temperature of the coating did not impact its hardness and did not result in stress relief or a reduction in misorientation.

4. Conclusion

This work confirms that the proposed duplex treatment is highly

beneficial for enhancing the properties of additively manufactured substrates, effectively addressing the limitations inherent to the printing process. Through the introduction of compressive residual stresses, this treatment mitigates the negative effect of build defects and tensile stresses on the material's fatigue life. Additionally, the increased substrate hardness enhances the coating's load-bearing capabilities, with the potential for further improvement by reducing the roughness induced by the peening treatment. This study thus contributes valuable insights into advancing the field of additive manufacturing and surface treatment for improved material performance.

Funding

We acknowledge the financial support for this research provided by the Ministry of Science and Technology (MOST) of the People's Republic of China (2019YFE0191500) and the Malta Council for Science (and Technology (MCST) through the Sino-Malta Fund 2019-02 (Science and Technology Cooperation) and the use of equipment purchased using the European Regional Development Funds: "Setting up of transdisciplinary research and knowledge exchange (TRAKE) complex at the University of Malta (ERDF.01.124)", which is being co-financed through the European Union through the European Regional Development Fund 2014–2020. The research work was also partially funded by the Endeavour II Scholarships Scheme, co-funded by the ESF+ 2021-2027.

CRediT authorship contribution statement

Kelsey Ann Vella: Data curation, Formal analysis, Investigation, Methodology, Validation, Writing – original draft, Writing – review & editing. **Joseph Buhagiar:** Resources, Supervision, Writing – review & editing. **Glenn Cassar:** Resources, Supervision, Writing – review & editing. **Bonnie Attard:** Methodology, Writing – review & editing. **Jian Chen:** Funding acquisition, Methodology, Project administration, Resources, Writing – review & editing. **Ann Zammit:** Conceptualization, Funding acquisition, Investigation, Methodology, Project administration, Supervision, Writing – review & editing.

Declaration of competing interest

The authors declare the following financial interests/personal relationships which may be considered as potential competing interests: Ann Zammit reports financial support was provided by Malta Council for Science and Technology. Jian Chen reports financial support was provided by Ministry of Science and Technology of the People's Republic of China. Ann Zammit, Glenn Cassar, Joseph Buhagiar, Luana Bonnici, Kelsey Ann Vella, Martina Pizzuto, Jian Chen, Xiyu Zhang, has patent #202210402564.2. Issued to Chinese National Patent. If there are other authors, they declare that they have no known competing financial interests or personal relationships that could have appeared to influence the work reported in this paper.

Data availability

Data will be made available on request.

References

[1] C. Leyens, M. Peters (Eds.), Titanium and Titanium Alloys: Fundamentals and Applications, first ed., . first ed., Wiley, 2003 https://doi.org/10.1002/3527602119.
[2] D.W. Chalmers, The properties and uses of marine structural materials, Mar. Struct. 1 (1) (1988) 47–70, https://doi.org/10.1016/0951-8339(88)90010-X. Jan.
[3] Z. Jianwen, Q. Henglei, Y. Jianchao, Z. Zhi, C. Tingting, L. Changliang, Q. Liang, S. Ying, O.Y. Wenbo, Y. Jian, S. Dan, The application and prospect of titanium materials in marine engineering equipments, in: Presented at the 12th World Conference on Titanium, 2011, pp. 2268–2271. Jun.
[4] I.V. Gorynin, A.S. Oryshchenko, V.P. Leonov, V.I. Mikhaylov, Titanium application in structures operating in sea water, in: Proceedings of the 12th World Conference on Titanium, 2011, pp. 2243–2248.
[5] B. Vrancken, L. Thijs, J.-P. Kruth, J. Van Humbeeck, Heat treatment of Ti6Al4V produced by selective laser melting: microstructure and mechanical properties, J. Alloys Compd. 541 (2012) 177–185, https://doi.org/10.1016/j.jallcom.2012.07.022. Nov.
[6] S. Liu, Y.C. Shin, Additive manufacturing of Ti6Al4V alloy: a review, Mater. Des. 164 (2019) 107552, https://doi.org/10.1016/j.matdes.2018.107552. Feb.
[7] E. Maleki, S. Bagherifard, M. Bandini, M. Guagliano, Surface post-treatments for metal additive manufacturing: progress, challenges, and opportunities, Addit. Manuf. 37 (2021) 101619, https://doi.org/10.1016/j.addma.2020.101619. Jan.
[8] A. Zammit, Shot peening of austempered ductile iron, in: M.A. Chowdhury (Ed.), Advanced Surface Engineering Research, IntechOpen, Rijeka, 2018, https://doi.org/10.5772/intechopen.79316.
[9] J.L. Daure, K.T. Voisey, P.H. Shipway, D.A. Stewart, The effect of coating architecture and defects on the corrosion behaviour of a PVD multilayer Inconel 625/Cr coating, Surf. Coat. Technol. 324 (2017) 403–412, https://doi.org/10.1016/j.surfcoat.2017.06.009. Sep.
[10] A. García, B. Rodríguez, H. Giraldo, Y. Quintero, R. Quezasa, N. Hassan, H. Estay, Copper-modified polymeric membranes for water treatment: a comprehensive review, Membranes 11 (2) (2021) 1–47, https://doi.org/10.3390/membranes11020093. Jan.
[11] A. Zammit, M. Attard, P. Subramaniyan, S. Levin, L. Wager, J. Cooper, L. Espitalier, G. Cassar, Enhancing surface integrity of titanium alloy through hybrid surface modification (HSM) treatments, Mater. Chem. Phys. 279 (2022) 125768, https://doi.org/10.1016/J.MATCHEMPHYS.2022.125768. Mar.
[12] A.A. Ahmed, M. Mhaede, M. Wollmann, L. Wagner, Effect of micro shot peening on the mechanical properties and corrosion behavior of two microstructure Ti–6Al–4V alloy, Appl. Surf. Sci. 363 (2016) 50–58, https://doi.org/10.1016/j.apsusc.2015.12.019. Feb.
[13] N. Tsuji, S. Tanaka, T. Takasugi, Effects of combined plasma-carburizing and shot-peening on fatigue and wear properties of Ti–6Al–4V alloy, Surf. Coat. Technol. 203 (10–11) (2009) 1400–1405, https://doi.org/10.1016/j.surfcoat.2008.11.013. Feb.
[14] B.K.C. Ganesh, W. Sha, N. Ramanaiah, A. Krishnaiah, Effect of shotpeening on sliding wear and tensile behavior of titanium implant alloys, Mater. Des. 1980-2015 56 (2014) 480–486, https://doi.org/10.1016/j.matdes.2013.11.052. Apr.
[15] K.A. Vella, J. Buhagiar, G. Cassar, M.M. Pizzuto, L. Bonnici, J. Chen, X. Zhang, Z. Huang, A. Zammit, The effect of a duplex surface treatment on the corrosion and tribocorrosion characteristics of additively manufactured Ti-6Al-4V, Materials 16 (5) (2023), https://doi.org/10.3390/ma16052098.
[16] Q. Zhang, S. Xu, J. Wang, X. Zhang, J. Wang, C. Si, Microstructure change and corrosion resistance of selective laser melted Ti-6Al-4V alloy subjected to pneumatic shot peening and ultrasonic shot peening, Surf. Topogr. Metrol. Prop. 10 (1) (2022), https://doi.org/10.1088/2051-672X/ac4c83. Mar.
[17] S.J. Lainé, K.M. Knowles, P.J. Doorbar, R.D. Cutts, D. Rugg, Microstructural characterisation of metallic shot peened and laser shock peened Ti–6Al–4V, Acta Mater. 123 (2017) 350–361, https://doi.org/10.1016/j.actamat.2016.10.044. Jan.
[18] Z. Zhang, D. Lin, S.L. Teo, F. Wei, H.R. Tan, A.K. Cheong, S.H. Lim, S. Wang, J. P an, Fatigue life enhancement in alpha/beta Ti–6Al–4V after shot peening: an EBSD and TEM crystallographic orientation mapping study of surface layer, Materialia 12 (2020) 100813, https://doi.org/10.1016/j.mtla.2020.100813.
[19] J. Lv, K. Luo, H. Lu, Z. Wang, J. Liu, J. Lu, Achieving high strength and ductility in selective laser melting Ti-6Al-4V alloy by laser shock peening, J. Alloys Compd. 899 (2022) 163335, https://doi.org/10.1016/j.jallcom.2021.163335. Apr.
[20] I. Yeo, S. Bae, A. Amanov, S. Jeong, Effect of laser shock peening on properties of heat-treated Ti–6Al–4V manufactured by laser powder bed fusion, Int. J. Precis. Eng. Manuf.-Green Technol. 8 (4) (2021) 1137–1150, https://doi.org/10.1007/s40684-020-00234-2. Jul.
[21] H. Lu, Z. Wang, J. Cai, X. Xu, K. Luo, L. Wu, J. Lu, Effects of laser shock peening on the hot corrosion behaviour of the selective laser melted Ti6Al4V titanium alloy, Corrosion Sci. 188 (2021) 109558, https://doi.org/10.1016/j.corsci.2021.109558. Aug.
[22] C. Zhang, M. Zheng, Y. Wang, P. Gao, B. Gan, Effect of high energy shot peening on the wear resistance of TiN films on a TA2 surface, Surf. Coat. Technol. 378 (2019), https://doi.org/10.1016/j.surfcoat.2019.07.045. Nov.
[23] A. Zammit, M. Attard, P. Subramaniyan, S. Levin, L. Wager, J. Cooper, L. Espitalier, G. Cassar, Investigations on the adhesion and fatigue characteristics of hybrid surface-treated titanium alloy, Surf. Coat. Technol. 431 (2022) 128002, https://doi.org/10.1016/j.surfcoat.2021.128002.
[24] N. Ravi, R. Markandeya, S.V. Joshi, Effect of substrate roughness on adhesion and tribological properties of nc-TiAlN/a-Si3N4 nanocomposite coatings deposited by cathodic arc PVD process, Surf. Eng. 33 (1) (2017) 7–19, https://doi.org/10.1179/1743294415Y.0000000005. Jan.
[25] J. Jiang, R.D. Arnell, The Effect of Substrate Surface Roughness on the Wear of DLC Coatings, 2000 [Online]. Available: www.elsevier.comrlocaterwear.
[26] Y.M. Wang, J.P. Cheng, H.P. Yang, C.H. Zhang, B.X. Wang, Influence of microstructure on shot peening effects of Ti-6Al-4V alloy, Mater. Sci. Forum 921 (2018) 177–183. https://doi.org/10.4028/www.scientific.net/MSF.921.177.
[27] Q. Yang, W. Zhou, Z. Niu, Z. Zheng, Q. Wang, X. Fu, G. Chen, Z. Li, Effect of different surface asperities and surface hardness induced by shot-peening on the fretting wear behavior of Ti-6Al-4V, Surf. Coat. Technol. 349 (2018) 1098–1106, https://doi.org/10.1016/J.SURFCOAT.2018.06.092. Sep.
[28] G. Cassar, A. Batista, J.C. Wilson, S. Banfield, J. Housden, A. Matthews, A. Leyland, A study of the reciprocating-sliding wear performance of plasma surface treated

titanium alloy, Wear 269 (2010) 60–70, https://doi.org/10.1016/j.wear.2010.03.008. May.
[29] C.T. Wang, T.J. Hakala, A. Laukkanen, H. Ronkainen, K. Holmberg, N. Gao, R.J. K. Wood, T.G. Langdon, An investigation into the effect of substrate on the load-bearing capacity of thin hard coatings, J. Mater. Sci. 51 (9) (2016) 4390–4398, https://doi.org/10.1007/s10853-016-9751-8. May.
[30] O. Çomaklı, Improved structural, mechanical, corrosion and tribocorrosion properties of Ti45Nb alloys by TiN, TiAlN monolayers, and TiAlN/TiN multilayer ceramic films, Ceram. Int. 47 (3) (2021) 4149–4156, https://doi.org/10.1016/J.CERAMINT.2020.09.292. Feb.
[31] C.J. Feng, X. Hu, Y.F. Jiang, Q. Zhao, Effects of Cu addition on microstructure and adhesion properties of Ti-Al-N nanocomposite films deposited by magnetron sputtering, Adv. Mater. Res. 652–654 (2013) 1751–1754. https://doi.org/10.4028/www.scientific.net/AMR.652-654.1751. Jan.
[32] D.S. Belov, I.V. Blinkov, V.S. Sergevnin, N.I. Smirnov, A.O. Volkhonskii, A. V. Bondarev, T.A. Lobova, Abrasive, hydroabrasive, and erosion wear behaviour of nanostructured (Ti,Al)N-Cu and (Ti,Al)N-Ni coatings, Surf. Coat. Technol. 338 (2018) 1–13, https://doi.org/10.1016/j.surfcoat.2018.01.066. Mar.
[33] L. Bonnici, J. Buhagiar, G. Cassar, K.A. Vella, J. Chen, X. Zhang, Z. Huang, A. Zammit, Additively manufactured 316L stainless steel subjected to a duplex peening-PVD coating treatment, Materials 16 (2) (2023), https://doi.org/10.3390/ma16020663.
[34] D. Zhang, L. Wang, H. Zhang, A. Maldar, G. Zhu, W. Chen, J.S. Park, J. Wang, F. Meng, Effect of heat treatment on the tensile behavior of selective laser melted Ti-6Al-4V by in situ X-ray characterization, Acta Mater. 189 (2020), https://doi.org/10.1016/j.actamat.2020.03.003. Mar.
[35] T. DebRoy, H.L. Wei, J.S. Zuback, T. Mukherjee, J.W. Elmer, J.O. Milewski, A. M. Beese, A. Wilson-Heid, A. De, W. Zhang, Additive manufacturing of metallic components – process, structure and properties, Prog. Mater. Sci. 92 (2018) 112–224, https://doi.org/10.1016/j.pmatsci.2017.10.001.
[36] S. Cao, Y.H. Zou, C.V.S. Lim, X. Wu, Review of laser powder bed fusion (LPBF) fabricated Ti-6Al-4V: process, post-process treatment, microstructure, and property, Light Adv. Manuf. (2021).
[37] Y. Hu, M. Lai, Z. Hu, Z. Yao, Effect of multiple laser peening on surface integrity and microstructure of laser additive manufactured Ti6Al4V titanium alloy, Rapid Prototyp. J. 25 (8) (2019) 1379–1387, https://doi.org/10.1108/RPJ-09-2018-0250. Sep.
[38] W. Chen, L. Xiao, Q. Sun, J. Sun, Effect of the initial grain size on grain refinement in Ti–2Al–2.5Zr alloy subjected to multi-impact process, Mater. Sci. Eng., A 554 (2012) 86–94, https://doi.org/10.1016/j.msea.2012.06.019.
[39] H. Gao, Y. Huang, Geometrically necessary dislocation and size-dependent plasticity, Scripta Mater. 48 (2) (2003) 113–118, https://doi.org/10.1016/S1359-6462(02)00329-9. Jan.
[40] C. Moussa, M. Bernacki, R. Besnard, N. Bozzolo, About quantitative EBSD analysis of deformation and recovery substructures in pure Tantalum, IOP Conf. Ser. Mater. Sci. Eng. 89 (2015) 012038, https://doi.org/10.1088/1757-899X/89/1/012038. Aug.
[41] A.K. Saxena, M. Anupoju, A. Tewari, P. Pant, Effect of grain size on deformation twinning behavior of Ti6Al4V alloy, in: Materials Science Forum, Trans Tech Publications Ltd, 2015, pp. 337–340. https://doi.org/10.4028/www.scientific.net/MSF.830-831.337.
[42] L. Xie, Y. Wen, K. Zhan, L. Wang, C. Jiang, V. Ji, Characterization on surface mechanical properties of Ti-6Al-4V after shot peening, J. Alloys Compd. 666 (2016) 65–70, https://doi.org/10.1016/j.jallcom.2016.01.119. May.